Morphogenesis of extra-embryonic tissues directs the remodelling of the mouse embryo at implantation

Neophytos Christodoulou[1,#], Antonia Weberling[1,#], Douglas Strathdee[2], Kurt I Anderson[3], Paul Timpson[4], and Magdalena Zernicka-Goetz[1*]

Affiliations:

[1] Mammalian Embryo and Stem Cell Group, University of Cambridge, Department of Physiology, Development and Neuroscience; Downing Street, Cambridge, CB2 3DY, UK

[2] Cancer Research UK Beatson Institute, Glasgow, United Kingdom.

[3] Francis Crick Institute, London, United Kingdom.

[4] Garvan Institute of Medical Research and The Kinghorn Cancer Centre, Cancer Division, Sydney, NSW 2010, Australia; St Vincent's Clinical School, Faculty of Medicine, University of NSW, Sydney, NSW 2010, Australia.

[#] These authors contributed equally.

*corresponding author: mz205@cam.ac.uk

Abstract

Mammalian embryos change shape dramatically upon implantation. The cellular and molecular mechanism underlying this transition are largely unknown. Here, we show that this transition is directed by cross talk between the embryonic epiblast and the first extra-embryonic tissue, the trophectoderm. Specifically, we show via visualisation of a Cdx2-GFP reporter line and pharmacologically mediated loss and gain of function experiments that the epiblast provides FGF signal that results in differential fate acquisition in the multipotent trophectoderm leading to the formation of a tissue boundary within the tissue. The trophectoderm boundary becomes essential for its expansion into a multi-layered epithelium. Folding of this multi-layered trophectoderm induces spreading of the second extra-embryonic tissue, the primitive endoderm. Together, these events remodel the pre-implantation embryo into its post-implantation cylindrical shape. Our findings uncover how communication between embryonic and extra-embryonic tissues provides positional cues to drive shape change in mammalian development during implantation.

Introduction

Before implantation, mammalian embryos consist of the embryonic epiblast and two extra-embryonic lineages, the trophectoderm (TE) and the primitive endoderm (PE)

organised into the hollow, spherical blastocyst. Upon implantation this simple structure becomes remodelled[1-5], in the case of the mouse embryo, into the so-called egg cylinder[3]. During this period, the pluripotent epiblast polarises and forms a central lumen[6] while maintaining its position relative to the extra-embryonic tissues.

In the blastocyst, the TE is subdivided into polar TE, which covers the epiblast at the embryonic pole, and mural TE, which overlays the blastocyst cavity at the abembryonic pole[7,8]. During implantation development, the polar TE remains multipotent and gives rise to the extra-embryonic ectoderm (ExE)[9], which will contribute to the embryonic part of the placenta [10]. The mural TE, on the other hand, differentiates into primary trophoblast giant cells, which are necessary for embryo implantation[11,12]. Blastocysts reconstituted by injecting epiblasts into trophospheres formed from isolated mural TE cells, can develop into post-implantation embryos[13-15]. Thus, the distinct behaviour of polar and mural TE has been proposed to result from differential signalling emanating from the epiblast [13-15].

The epiblast expresses FGF ligands during implantation development[16]. It has been suggested that such FGF signalling is necessary for post-implantation TE development because the isolation and maintenance of trophoblast stem cells in culture depends upon FGF4 to sustain its multipotent character[17]. However, in addition to its role in trophoblast stem cell maintenance, FGF signalling is necessary for pre-implantation development[18] as it controls primitive endoderm specification[19-23]. Specifically, FGF4 expressed by the ICM signals through FGFR1 and FGFR2 to promote and maintain the expression of primitive endoderm lineage markers[24-26]. Consequently, knock out mice for FGFR1,2 and FGF4 display pre-implantation phenotypes due to impaired PE specification[18,25-27] and so the role of FGF signalling in TE morphogenesis during implantation development has remained unclear.

Here, we demonstrate that FGF ligands produced by the epiblast are necessary for maintenance of trophectoderm multipotency and the differential fate acquisition of polar and mural trophectoderm, which leads to the establishment of a tissue boundary at the polar/mural trophectoderm interface. We show that the formation of this tissue boundary is indispensable for embryogenesis as its inhibition leads to defective polar trophectoderm expansion into the extra-embryonic ectoderm. Last, we demonstrate that newly formed extra-embryonic ectoderm folds, resulting in cell shape changes driven spreading of the primitive endoderm. These results demonstrate how morphogenesis of the extra-embryonic tissues drive the remodelling of the mouse embryo during implantation.

Results

Trophectoderm cell flow ceases upon implantation

The pre-implantation blastocyst comprises three distinct tissues spatially distributed along the embryonic-abembryonic axis: the embryonic (Em) pole comprises the epiblast surrounded by the polar TE and the PE while the abembryonic (Ab) pole consists of the mural TE encompassing the blastocyst cavity (Figure 1a). Upon implantation, the spherically-shaped blastocyst transforms into the egg cylinder. During this process, the polar TE generates the extra-embryonic ectoderm (ExE). This is followed by formation of visceral endoderm (VE) from the PE and its spreading to cover both epiblast and ExE (Figure 1a-c). It is known that before its expansion, the polar TE exhibits a flow towards the mural TE, leading to an increase in mural TE cell population[9,28-30]. Since such a polar to mural flow of the TE is not compatible with expansion of the polar TE in the opposite direction to form the ExE, we hypothesised that the polar TE cell flow must be terminated to allow ExE formation. To test this hypothesis, we filmed developing blastocysts expressing Cdx2-GFP to visualise the TE at two developmental stages (Figure 1d-i, Supplementary Figure 1a-c, Supplementary Movie 1-3). Analysis of individual cell behaviour in pre-implantation blastocysts revealed the polar to mural TE flow (Figure 1d-g, Supplementary Figure 1a, Supplementary Movie 1), which was terminated in implanting blastocysts (Figure 1h-j, Supplementary Figure 1b-c, Supplementary Movie 2-3). Interestingly, we noticed that as the polar to mural TE flow stopped, a gradient of Cdx2, indicative of TE potency[31], became established with higher levels of Cdx2 on the polar side than on the mural side (Supplementary Figure 1b, Supplementary Movie3). This gradient of Cdx2 expression was evident only upon termination of the flow and not before implantation when the polar to mural TE flow was taking place (Supplementary Figure 1d). These results suggest that differential properties of polar and mural TE regulate polar TE cell flow during implantation.

Trophectoderm tissue boundary forms during implantation

We next sought to determine how the termination of the polar to mural TE flow is achieved. In various systems, cell populations with different fates and function become separated by the formation of tissue boundaries. These are characterised by high actomyosin contractility at the respective interface of the two populations to prevent cell mixing[32-36]. To investigate whether the differentiation within the TE results in the generation of such a boundary between polar and mural parts, we analysed the distribution of actomyosin during and after

termination of the flow. We found high actomyosin contractility at the interface between TE cells expressing Cdx2 at high and low levels (Figure 2a-b, Supplementary Figure 2).

As cell-cell-junction angles are known to undergo a characteristic widening upon tissue boundary formation[37], we measured the angles between cells at the putative boundary within the TE. This revealed how the angles between cell junctions increased as the entire boundary became linear (Figure 2c-d, Supplementary Movie 4). These results indicate that a tissue boundary becomes established between polar and mural parts of the TE when the blastocyst initiates its transformation into the egg cylinder.

Polar trophectoderm expansion follows tissue boundary formation

To determine the dynamics of polar/mural TE boundary formation and polar TE expansion to form the ExE, we filmed the development of blastocysts recovered from the mother at the time of implantation (E4.5). We observed that polar TE expansion occurred after tissue boundary formation (Figure 3a, Supplementary Movie 5). In support of this, we observed cell shape changes in the TE once cell-cell junction angles increased. Whereas in early implanting blastocysts, polar TE cells were squamous, they transformed first into cuboidal and then columnar cells exhibiting reduced apical cell area following the polar/mural TE boundary formation (Figure 3b-c, Supplementary Figure 3a-b). During the same developmental period, the density of polar TE cells increased (Supplementary Figure 3c). Upon acquisition of columnar shape, polar TE cells changed the orientation of their division planes (Figure 3d-f, Supplementary Movie 6). Before tissue boundary formation and for as long as the polar TE epithelium remained single-layered, these cells divided perpendicular to the Em/Ab axis of the embryo and parallel to the epithelial layer (Figure 3f, Supplementary Figure 3d, Supplementary Movie 2-4). In contrast, once the tissue boundary formed and the cells had acquired columnar morphology, they divided along their long axes and therefore parallel to the Em/Ab axis and perpendicular to the epithelial layer. This resulted in expansion of the polar TE into a multi-layered epithelium (Figure 3d-f, Supplementary Movie 6). These observations suggest that the formation of a polar/mural TE boundary correlates with expansion of the polar TE into the ExE during egg cylinder morphogenesis.

FGF and actomyosin control tissue boundary formation

It has been proposed that positional information provided by the epiblast might be responsible for the differentiation into polar and mural TE, because only the polar but not the

mural TE is in direct contact with the epiblast[13,14,38]. FGF signalling is necessary for the maintenance of trophoblast stem cell character and is active in the ExE, which forms from the polar TE in early post-implantation stages[17,27,39]. At the time of implantation, the epiblast expresses FGF ligands[16,40,41], mainly FGF4 and FGF5 (Supplementary Figure 4a), while the TE expresses FGF receptors (FGFR1, 2)[25,42,43]. Therefore, we hypothesised that maintenance of Cdx2 expression in the polar TE at the time of implantation could be a response of the tissue to FGF signalling. To test this possibility, we first assessed the status of FGF signalling before and during implantation using p-ERK and p-AKT as a read out of its activity[39,44]. This revealed that FGF signalling was not active in the polar TE before implantation but showed restricted activation in the polar TE in implanting blastocysts (Figure 4a-b, Supplementary Figure 4b-c).

To examine whether FGF signalling is indeed responsible for the maintenance of multipotency in the polar TE at implantation stages, we inhibited FGF signalling in *ex-vivo* cultured blastocysts through treatment with a specific FGF receptor inhibitor[39] for 20 h (Figure 4c). This treatment gave us temporal control over FGF inhibition and avoided an effect on the earlier specification of PE[18,21,25-27]. Inhibition of FGF signalling resulted in the loss of Cdx2 expression in the polar TE (Supplementary Figure 4d) without affecting specification of PE, which was already formed by the time of treatment. To confirm the role of FGF in differentially affecting the polar and mural TE, we next recovered blastocysts at E3.5 and cultured them for 24h to the E4.5 stage before treating them with FGF for 24h. This revealed that the presence of FGF prevents mural TE differentiation as indicated by Cdx2 expression levels (Supplementary Figure 5a-c). These results indicate that positional information from the epiblast in the form of FGF signalling is responsible for the maintenance of multipotency in the polar TE, evident from the appearance of a gradient in Cdx2 expression.

Since we observed high actomyosin contractility at the interface of polar/mural TE and as FGF signalling is responsible for multipotency maintenance in the polar TE resulting in the appearance of a Cdx2 expression gradient in the TE, we next wished to determine whether actomyosin contractility and FGF signalling play a role in the formation of the boundary between polar and mural TE. To this end, we cultured E4.5 blastocysts for 20h in the presence of ROCK inhibitor or blebbistatin(-) to inhibit actomyosin contractility[45] (Figure 4c, Supplementary Figure 6a). Inhibition of actomyosin contractility resulted in significantly

narrowed angles of the cell-cell borders at the polar/mural TE interface indicative of defective boundary formation (Figure 4d-f, Supplementary Figure 6b-c), thus confirming the essential role of actomyosin contractility in this process. Similarly, inhibition of FGF signalling during the same developmental time window led to defective polar/mural TE boundary formation (Figure 4d-f). Together, these results indicate the necessity of FGF signalling from the epiblast to the polar TE for the formation of the tissue boundary between polar and mural TE.

To understand the role of the mural/polar TE boundary in subsequent development, we perturbed its formation by inhibiting either FGF signalling or actomyosin contractility in implanting embryos and following their subsequent development. We found that inhibition of FGF signalling or actomyosin contractility led to failure of both the polar TE to expand to form the ExE and egg cylinder formation (Figure 4g-h, Supplementary Figure 6b,d)). These results indicate that formation of the polar/mural TE tissue boundary is a key step in blastocyst to egg cylinder morphogenesis (Figure 4i).

Primitive endoderm morphogenesis

During the final stage of the blastocyst to egg cylinder transformation, the PE differentiates into the VE, which will cover both the epiblast and the newly formed ExE (Figure 1a-c). To gain insight into this process, we analysed the behaviour of the PE at consecutive stages of implantation development *in vivo* and *in vitro*. We found that PE cells localised at the distal tip of the epiblast facing the blastocyst cavity displayed a cuboidal shape, which became columnar upon implantation while still confined to the distal tip (Figure 5a-b, Supplementary Figure 7a-b, Supplementary Figure 8, Supplementary Movie 7). However, as development progressed, PE cells changed shape again to become cuboidal, concomitant with their spreading over the epiblast and the expansion of the polar TE (Figure 5a-c, Supplementary Figure 7b, Supplementary Figure 8-9, Supplementary Movie 7). These results suggest that expansion of the polar TE and spreading of the PE/VE are coordinated events.

During implantation development, the PE gives rise not only to the VE but also to the parietal endoderm[46]. The parietal endoderm migrates towards the mural TE with Reichert's membrane acting as a substrate for its migration[47]. Since it is possible that parietal endoderm migration might also contribute to PE morphogenesis during implantation development, we examined the movement of parietal endoderm cells in implanting blastocysts (E4.5-E4.75).

We found that parietal endoderm migration is completed before the TE expands and the PE spreads over the epiblast (Figure 5d). These results strongly suggest that parietal endoderm migration is not involved in PE/VE morphogenesis.

Immediately preceding egg cylinder formation, the PE covers only the epiblast and is not in contact with the polar TE (Figure 5a-b, Supplementary Figure 8,9). We hypothesised that the polar TE expansion into ExE might act as a substrate for migration of the PE to cover the ExE. This would require degradation of the Reichert's membrane that encloses the distal half of the embryo forming a continuous membrane with the embryonic basement membrane (Figure 5e upper panel). However, we found that after spreading of the PE, the whole egg cylinder remained enclosed by the continuous embryonic and Reichert's basement membrane (Figure 5e lower panel). Together, these observations suggest that active migration of PE cells is not required for egg cylinder formation.

Trophectoderm folding results in egg cylinder formation

To understand how the PE develops into the VE, which covers the entire embryo during egg cylinder formation, we performed live imaging of Lifeact-GFP transgenic embryos from an early post-implantation stage (E4.75). Analyses of our movies revealed that the VE spreads over the ExE concomitantly with the folding of the ExE (Figure 6a-f, Supplementary Figure 8-1 0, Supplementary Movie 8-9). Examination of embryos developing *in vivo* and fixed immediately upon recovery demonstrated that ExE folding is followed by directional growth of the embryo towards the Ab pole of the blastocyst cavity, which results in filling of the previously hollow space (Supplementary Figure 9).

Based on the above observations we hypothesised that ExE folding could be the driving force for VE morphogenesis. Specifically, we considered that ExE folding and embryo movement towards the Ab pole might lead to the development of stretching forces leading to cell shape driven spreading of the VE[48]. To test this hypothesis, we measured the orientation of the long axes of VE cells and found that, upon ExE folding, the most proximal cells of the VE became aligned with the proximo-distal axis of the embryo (Figure 6g, Supplementary Figure 9). These results suggest the possibility that the VE responds passively to tensile forces[48-50] generated along the proximal-distal axis as a result of ExE invagination.

To test this possibility further, we sought to prevent the ExE folding, which requires apical constriction[51] and so can be prevented using a ROCK inhibitor[45]. We found that ROCK inhibition applied from an early post-implantation stage (E4.75), resulted in failure of ExE invagination, VE spreading, and consequently egg cylinder formation (Figure 6h-i, Supplementary Figure 11a, Supplementary Movie 10). To exclude any contribution of active VE cell movement as it develops to cover the ExE, we inhibited Rac, which is indispensable for collective cell migration[52,53], and filmed the subsequent development. Inhibition of Rac affected neither expansion of the VE to cover the epiblast and ExE nor egg cylinder formation (Supplementary Figure 11b), in accord with the phenotype of embryos that are Rac1 knock-out only in the VE[52]. Thus, the expansion of the VE appears to be a passive response to egg cylinder formation.

Discussion

In this study, we describe morphogenetic events driving the critical phase of mammalian embryo development that takes place during implantation. Our findings demonstrate an interplay between positional, chemical signals and physical cellular responses that leads to global tissue rearrangements as the mouse blastocyst transforms into the egg cylinder. Specifically, we describe how FGF signalling from the epiblast determines the fate of a subset of TE cells and subsequent morphogenesis that generates forces necessary for the spreading of the PE/VE to cover not only the epiblast but also the expanding ExE (Figure 6j).

Here, we show that the first morphogenetic event during the blastocyst to egg cylinder transition is the formation of a tissue boundary between the polar and mural TE. Formation of this boundary prevents the flow of polar TE cells towards the mural region that occurs at pre-implantation stages. Abrogation of the formation of the TE boundary shows that it is necessary for proper embryo development. Our results show that actomyosin contractility at the interface between the mural and polar TE is indispensable for tissue boundary formation. Such an increase in actomyosin contractility at the interface of differentially fated cells is a feature of tissue boundary formation in various model systems[54]. In the case of the polar/mural TE boundary, the localised increase of actomyosin contractility at the interface could either be a result of heterophilic adhesions [32,37] or repulsive cues generated by Ephrin/Eph signalling[55,56].

Numerous studies have described the role of FGF signalling in PE specification and in the maintenance of trophoblast stem cells[17,18,21,25-27,41]. However how FGF signalling instructs the peri-implantation morphogenesis of the TE has not previously been studied due to the pre-implantation phenotypes of FGF and FGFR knock-out embryos[18,25,26]. Here, we show that the TE tissue boundary forms in response to FGF signalling originating from the epiblast. Specifically, FGF ligands produced by the epiblast act as positional cues driving differential fate acquisition of the polar (undifferentiated) and mural (differentiated) TE. Importantly, whereas FGF signalling is indispensable for polar TE morphogenesis and multipotency maintenance upon implantation, it is dispensable for maintenance of the TE's multipotent state in pre-implantation stages[25,41]. During pre-implantation development, TE multipotency is maintained by co-operation of Notch and Hippo pathways[57-59]. It will be important to identify the mechanisms controlling the switch from FGF-independent to FGF-dependent maintenance of TE multipotency during peri-implantation development in future studies.

Upon TE tissue boundary formation, polar TE cells change from squamous to columnar morphologies. Similar shape changes from squamous to columnar morphologies are evident in the PE during egg cylinder formation. This could result from cell crowding due to continuous cell proliferation in a restricted environment[48,60]. Polar TE cells divide in a confined area imposed upon them by the formation of the tissue boundary between themselves and the mural TE. The PE tissue increases its cell number while being confined to the distal site of the epiblast. Polar TE cell shape changes are followed by polarised cell divisions that both contribute to the formation of the double cell layer of the ExE. TE expansion is followed by PE spreading over the epiblast, during which the PE cells change their shape from columnar to cuboidal. These cell shape changes could be a result of stretching forces experienced by the PE during TE expansion and the movement of the epiblast towards the abembryonic pole of the implanting blastocyst[48].

The final step of egg cylinder formation is orchestrated by invagination of the newly formed ExE, which is driven by apical constriction of ExE cells[51]. Apical constriction as a mechanism for tissue folding has been described in different models[61-64]. Here, folding is initiated by apical constriction only when the polar TE expands to form the ExE. The proliferation of polar TE during this process leads to an increased cell density, which correlates with an increase in pressure forces within epithelial tissues[65]. It has been reported

that mechanical signals regulate myosin II distribution and turnover during tissue morphogenesis and wound healing[66-68]. Thus, we hypothesise that initiation of ExE folding as a result of apical constriction might be regulated by mechanically mediated enrichment of myosin II through a mechano-transductive cascade.

Our results demonstrate that ExE folding is followed by VE spreading over the ExE, which is necessary for the completion of the blastocyst to egg cylinder transition. We find that neither parietal endoderm migration nor active PE cell migration contribute to this process. Just as with the spreading of PE over the epiblast, the spreading of VE over the ExE is probably driven by mechanically induced cell shape changes[48]. In this case, the force generating mechanism is the folding of the ExE, which results in the directional growth of the embryo towards the Ab pole[9]. In agreement, prevention of ExE folding by inhibition of apical constriction results in impaired egg cylinder formation and VE spreading.

In summary, our results demonstrate that TE morphogenesis orchestrates the shape acquisition of the post-implantation mouse embryo during the blastocyst to egg cylinder transition. The fact that murine and primate embryos are similar in morphology to the time of implantation, when they begin to display differential behaviour of the TE [1-5], suggests that the different shapes of murine and primate post-implantation embryos might be attributed to TE peri-implantation morphogenesis. Future studies on TE morphogenesis in different species should shed light onto the role of the TE in the mechanisms that lead to the characteristic shapes of implantation embryos of different mammalian species.

Methods

Embryo Recovery and Culture

In accordance with national and international guidelines, the mice used were kept in the animal facility. All experiments performed have been regulated by the Animals (Scientific Procedures) Act 1986 Amendment Regulations 2012 and additional ethical review by the University of Cambridge Animal Welfare and Ethical Review Body (AWERB). Experiments were authorised by the Home Office (Licence number: 70/8864). Upon any identification of health concern, mice were culled by cervical dislocation. Pre-implantation stage embryos from Cdx2-GFP transgenic or CD1 females mated with either Cdx2-GFP

transgenic, F1, MF1, or CD1 males were flushed from the uteri and cultured in KSOM. Peri-implantation and early post-implantation embryos from Pdgfra-GFP, Lifeact-GFP, E-Cadherin-GFP, Cdx2-GFP, and CD1 females mated with either Pdgfra-GFP, LIFEACTT-GFP, E-Cadherin-GFP, Cdx2-GFP, F1, MF1, and CD1 males were dissected from the uteri or deciduas and cultured in drops of Advanced DMEM/F12 (GIBCO) containing 20% FBS and supplemented with 2 mM L-glutamine (GIBCO), 1 mM sodium pyruvate (GIBCO), penicillin (25 units/ml)/streptomycin (25 μg/ml) (GIBCO), 1 × ITS-X (Invitrogen). The medium drops were covered with mineral oil and the embryos were cultured at 37ºC and 5% CO_2.

For ROCK inhibition, the embryos were placed in drops of medium, either containing Y-27632 ROCK inhibitor (100 μM) dissolved in DMSO or solely DMSO as a control and incubated 20 hours for examination of tissue boundary formation and 12 hours for examination of ExE folding at the above described conditions. For blebbistatin(-) treatment, the embryos were placed in drops of medium, either containing 50 μM blebbistatin(-) dissolved in DMSO or solely DMSO as a control and incubated 20 hours for examination of tissue boundary formation at the above described conditions. For FGF treatment, embryos were recovered at E3.5 cultured for 24h in KSOM and then cultured for another 24h in IVC medium in the presence or the absence of 1000ng/ml Fgf4 + 1ug/ml Heparin FGFR inhibition was achieved through incubation of blastocysts in medium containing SU5402 at 40 μM or DMSO for the control group. For Rac inhibition, Rac1 Inhibitor II, Z62954982 at a concentration of 100 μM was used and embryos for the control group were incubated in the same amount of DMSO.

Generation of endogenous E-Cadherin-GFP transgenic mouse line

A Cdh1-EGFP allele was created by inserting a loxP-stop-loxP-EGFP cassette immediately prior to the endogenous stop codon in the final exon of the Cdh1 gene (ENSMUSE00000469626; Chromosome 8: 106,668,613). The allele was designed that following Cre recombination the stop codon was removed and the EGFP open reading frame was fused to the coding sequence of the Cdh1 gene creating a Cdh1-EGFP fusion protein. Prior to Cre recombination the loxP sites are separated by 300bp spacer sequence composed of non-coding sequence from the human Pgk1 gene.

The targeting vector was assembled as follows. Two synthetic DNA fragments (MWG Eurofins) were ligated to form a combined fragment comprising 5' (300bp) and 3' (500bp)

Cdh1 homology arms flanking a loxP-STOP-loxP element immediately adjacent to the last amino acid codon of Cdh1, an EGFP open reading frame and a FRT site within the sequence of the Cdh1 3' UTR.

An FRT-Hygro-R cassette was inserted into the above plasmid by co-transfection into EL250 *E.coli* [69]which express Flp recombinase under arabinose induction.

The DNA fragment bound by the homology arms was excised and recombined[69] into a pool of mouse genomic DNA BAC clones (Source Biosciences) carrying the mouse Cdh1 gene in EL250 *E.coli*[70].

A retrieval plasmid was generated by cloning a retrieval fragment (comprising 540bp and 490 bp homology arms separated by a SwaI site) into NotI-AscI linearised pFlexDTA (a modified version of pFlexible)[71]. Following linearization by SwaI, the modified sequences were retrieved from BAC clones in EL250 *E.coli* by recombining. The retrieved plasmid represents the targeting vector with approximately 5kb and 4.5kb homology arms.

The targeting vector was linearised by AscI digestion and transfected into HM1 mESCs[72]. Cells were selected under hygromycin (150ug/ml) and surviving colonies picked and screened for targeting by long range PCR (using the Roche Expand Long Template PCR System) from within the STOP element or hygromycin-resistance cassette to sequences beyond the ends of the homology arms. Oligo sequences used to screen cells to ensure appropriate targeting of the Cdh1 gene were TACCACGTGGATACCCCAAG and AGGTATGCCAGAAGCCACAG for the 5' side and GTCCGAGGGCAAAGGAATAG and GAAGCCTCAGGTTTGGTTCC for the 3' side.

Following identification of correctly targeted clones, mouse lines were derived by injection of ES cells into C57BL/6J blastocysts. After breeding of chimeras, germline offspring were identified by coat colour and the presence of the modified allele was confirmed with the 3' loxP primers described above. Mice were subsequently crossed with a mouse line expressing Flpe (Tg(ACTFLPe)9205Dym) to delete the selectable marker by recombination at the FRT sites[73].

Immunostaining

Embryos were fixed directly following dissection in 4% paraformaldehyde (PFA) in PBS for 20 min at room temperature (RT). Incubation except fixation was carried out in wells coated with filtered FCS to avoid attachment of peri-implantation stages at the bottom of the wells. Permeabilisation was carried out for 20 min at RT through incubation in 0.3% Triton X-100 /

0.1M Glycin in PBS. Primary antibodies were prepared in blocking solution (0.1% Tween-20 / 10% filtered FCS in PBS) and incubated at 4ºC overnight. Secondary antibody incubation was performed at RT for 3h and carried out in blocking solution as well. Nuclear staining was incubated simultaneously with secondary antibodies using DAPI (10mg/ml). All washes were carried out in PBS supplemented with 0.1% Tween-20. For pERK staining, embryos were fixed in Methanol and incubated for 15 min at -20ºC in ice-cold Methanol. Following fixation, the embryos were stained as described above. Primary antibodies used: Cdx2 (mouse monoclonal, 1:300, Launch Diagnostics, MU392-UC (Biogenex); E-Cadherin (rat, 1:200, Thermo Fisher Scientific, 13-1900); Gata6 (goat, 1:200, R&D Systems, AF1700,); Laminin (rabbit, 1:300, Sigma, L9393); pAKT (rabbit, 1:100, Cell Signaling Technology, 4060T), pERK (rabbit, 1:100, New England Biolabs, 4377T); phospho-Myosin Light chain II (rabbit, 1:100, Cell Signaling Technology, 3671S), podocalyxin (1:300; R&D systems, MAB1556).

Secondary antibodies used:
Alexa Fluor® 488 Phalloidin (1:500, Thermo Fisher Scientific, A12379); Alexa Fluor® 594 Phalloidin (1:500, Thermo Fisher Scientific, A12381); Goat anti-Rat IgG (H+L) Secondary Antibody, Alexa Fluor 647 (donkey, 1:500, Thermo Fisher Scientific, A-21247); Alexa Fluor® 568 Donkey Anti-mouse IgG (donkey, 1:500, Thermo Fisher Scientific, A10037); Donkey anti-Mouse IgG (H+L) Secondary Antibody, Alexa Fluor® 488 (donkey, 1:500, Thermo Fisher Scientific, A-21202); Alexa Fluor 568 Donkey Anti-Rabbit IgG Antibody (donkey, 1:500, Thermo Fisher Scientific, A10042); Alexa Fluor® 647 Donkey Anti-Rabbit IgG (H+L) Antibody (donkey, 1:500, Thermo Fisher Scientific, A-31573); Alexa Fluor 647 Donkey Anti-Mouse IgG (H L) Antibody (donkey, 1:500, Thermo Fisher Scientific; A31571); Donkey anti-Rat IgG (H+L) Secondary Antibody, Alexa Fluor® 488 conjugate (donkey, 1:500, Thermo Fisher Scientific, A-21208)

Imaging

Fixed embryos were imaged on a Leica SP8 microscope using a 63x oil objective. Pre-implantation live blastocysts were imaged on a Spinning Disc 40x objective at a z-step size of 1 µm. Implanting blastocysts as well as early post-implantation embryos were imaged on a Leica multiphoton SP8 microscope using a 25x water objective with a z-step size of 1 µm. For excitation, a 488 nm laser was used. Embryos transgenic for Cdx2-GFP, E-Cadherin-

GFP, and Pdgfra-GFP were imaged with 1.5% of 488 nm laser. Embryos expressing LifeAct-GFP were imaged at 0.25% of 488 nm laser.

A detailed list of the reagents and equipment used for embryo mounting and culture to optimise live imaging is provided in the supplementary methods. A detailed protocol is uploaded in Nature protocol exchange (ref 74).

Image processing and analysis

Image analysis of fixed embryos was carried out using the Leica 3D viewer and Fiji. For single cell tracking, the Imaris image analysis software was used. Image processing was performed with the Fiji image processing software.

Statistics and Reproducibility

GraphPad Prism 6.0 software was used for all statistical analysis performed on the results obtained. For treatments, the embryos were allocated randomly to treatment and control group, but investigators were not blinded to group allocation. The sample size of the experiments carried out was defined based on previous experimental experience. Quantitative data presented, shows the mean ± s.e.m., percentages, or the total number of datapoints obtained. The statistical tests carried out on the quantitative data obtained are annotated in each figure legend. Except annotated otherwise, each experiment shown was carried out at least three times.

Data availability

The authors declare that all data supporting the findings of this study are available within the article and its supplementary information files or from the corresponding author upon reasonable request.

The source data of Figures 1d, 1h, 1i, 2c, 3a, 3d, 5c, 6a, and Supplementary Figures S1b, S7a, S10c-d, S11a can be found as supplementary movies. The complete data supporting the results discussed in this study are available upon a reasonable request from the corresponding author. The source data underlying Figures 2d, 3b, 3c, 3f, 4f, 5b, 6b-g, and Supplementary Figures 3c, 5b, and 10c are provided as a Source Data file.

References

1 Hertig, A. T., Rock, J. & Adams, E. C. A description of 34 human ova within the first 17 days of development. *Am J Anat* **98**, 435-493 (1956).
2 Luckett, W. P. The development of primordial and definitive amniotic cavities in early Rhesus monkey and human embryos. *Am J Anat* **144**, 149-167, (1975).
3 Smith, L. J. Embryonic axis orientation in the mouse and its correlation with blastocyst relationships to the uterus. Part 1. Relationships between 82 hours and 4 1/4 days. *J Embryol Exp Morphol* **55**, 257-277 (1980).
4 Shahbazi, M. N. *et al.* Self-organization of the human embryo in the absence of maternal tissues. *Nat Cell Biol* **18**, 700-708 (2016).
5 Shahbazi, M. N. & Zernicka-Goetz, M. Deconstructing and reconstructing the mouse and human early embryo. *Nat Cell Biol* **20**, 878-887 (2018).
6 Bedzhov, I. & Zernicka-Goetz, M. Self-organizing properties of mouse pluripotent cells initiate morphogenesis upon implantation. *Cell* **156**, 1032-1044 (2014).
7 Chavez, D. J., Enders, A. C. & Schlafke, S. Trophectoderm cell subpopulations in the periimplantation mouse blastocyst. *J Exp Zool* **231**, 267-271 (1984).
8 Rassoulzadegan, M., Rosen, B. S., Gillot, I. & Cuzin, F. Phagocytosis reveals a reversible differentiated state early in the development of the mouse embryo. *EMBO J* **19**, 3295-3303 (2000).
9 Copp, A. J. Interaction between inner cell mass and trophectoderm of the mouse blastocyst. II. The fate of the polar trophectoderm. *J Embryol Exp Morphol* **51**, 109-120 (1979).
10 Simmons, D. G. & Cross, J. C. Determinants of trophoblast lineage and cell subtype specification in the mouse placenta. *Dev Biol* **284**, 12-24 (2005).
11 Sutherland, A. Mechanisms of implantation in the mouse: differentiation and functional importance of trophoblast giant cell behavior. *Dev Biol* **258** 241-251 (2003).
12 Hu, D. & Cross, J. C. Development and function of trophoblast giant cells in the rodent placenta. *Int J Dev Biol* **54**, 341-354 (2010).
13 Gardner, R. L. & Johnson, M. H. An investigation of inner cell mass and trophoblast tissues following their isolation from the mouse blastocyst. *J Embryol Exp Morphol* **28**, 279-312 (1972).
14 Gardner, R. L., Papaioannou, V. E. & Barton, S. C. Origin of the ectoplacental cone and secondary giant cells in mouse blastocysts reconstituted from isolated trophoblast and inner cell mass. *J Embryol Exp Morphol* **30**, 561-572 (1973).
15 Papaioannou, V. E. Lineage analysis of inner cell mass and trophectoderm using microsurgically reconstituted mouse blastocysts. *J Embryol Exp Morphol* **68**, 199-209 (1982).
16 Boroviak, T. *et al.* Lineage-Specific Profiling Delineates the Emergence and Progression of Naive Pluripotency in Mammalian Embryogenesis. *Dev Cell* **35**, 366-382 (2015).
17 Tanaka, S., Kunath, T., Hadjantonakis, A. K., Nagy, A. & Rossant, J. Promotion of trophoblast stem cell proliferation by FGF4. *Science* **282**, 2072-2075 (1998).
18 Feldman, B., Poueymirou, W., Papaioannou, V. E., DeChiara, T. M. & Goldfarb, M. Requirement of FGF-4 for postimplantation mouse development. *Science* **267**, 246-249 (1995).

19 Chazaud, C., Yamanaka, Y., Pawson, T. & Rossant, J. Early lineage segregation between epiblast and primitive endoderm in mouse blastocysts through the Grb2-MAPK pathway. *Dev Cell* **10**, 615-624 (2006).
20 Nichols, J., Silva, J., Roode, M. & Smith, A. Suppression of Erk signalling promotes ground state pluripotency in the mouse embryo. *Development* **136**, 3215-3222 (2009).
21 Yamanaka, Y., Lanner, F. & Rossant, J. FGF signal-dependent segregation of primitive endoderm and epiblast in the mouse blastocyst. *Development* **137**, 715-724 (2010).
22 Kang, M., Piliszek, A., Artus, J. & Hadjantonakis, A. K. FGF4 is required for lineage restriction and salt-and-pepper distribution of primitive endoderm factors but not their initial expression in the mouse. *Development* **140**, 267-279 (2013).
23 Krawchuk, D., Honma-Yamanaka, N., Anani, S. & Yamanaka, Y. FGF4 is a limiting factor controlling the proportions of primitive endoderm and epiblast in the ICM of the mouse blastocyst. *Dev Biol* **384**, 65-71 (2013).
24 Ohnishi, Y. *et al.* Cell-to-cell expression variability followed by signal reinforcement progressively segregates early mouse lineages. *Nat Cell Biol* **16**, 27-37 (2014).
25 Molotkov, A., Mazot, P., Brewer, J. R., Cinalli, R. M. & Soriano, P. Distinct Requirements for FGFR1 and FGFR2 in Primitive Endoderm Development and Exit from Pluripotency. *Dev Cell* **41**, 511-526 e514 (2017).
26 Kang, M., Garg, V. & Hadjantonakis, A. K. Lineage Establishment and Progression within the Inner Cell Mass of the Mouse Blastocyst Requires FGFR1 and FGFR2. *Dev Cell* **41**, 496-510 e495 (2017).
27 Goldin, S. N. & Papaioannou, V. E. Paracrine action of FGF4 during periimplantation development maintains trophectoderm and primitive endoderm. *Genesis* **36**, 40-47 (2003).
28 Copp, A. J. Interaction between inner cell mass and trophectoderm of the mouse blastocyst. I. A study of cellular proliferation. *J Embryol Exp Morphol* **48**, 109-125 (1978).
29 Cruz, Y. P. & Pedersen, R. A. Cell fate in the polar trophectoderm of mouse blastocysts as studied by microinjection of cell lineage tracers. *Dev Biol* **112**, 73-83 (1985).
30 Gardner, R. L. Flow of cells from polar to mural trophectoderm is polarized in the mouse blastocyst. *Hum Reprod* **15**, 694-701 (2000).
31 Strumpf, D. *et al.* Cdx2 is required for correct cell fate specification and differentiation of trophectoderm in the mouse blastocyst. *Development* **132**, 2093-2102 (2005).
32 Dahmann, C., Oates, A. C. & Brand, M. Boundary formation and maintenance in tissue development. *Nat Rev Genet* **12**, 43-55, doi:10.1038/nrg2902 (2011).
33 Monier, B., Pelissier-Monier, A., Brand, A. H. & Sanson, B. An actomyosin-based barrier inhibits cell mixing at compartmental boundaries in Drosophila embryos. *Nat Cell Biol* **12** (2010).
34 Canty, L., Zarour, E., Kashkooli, L., Francois, P. & Fagotto, F. Sorting at embryonic boundaries requires high heterotypic interfacial tension. *Nat Commun* **8**, 157 (2017).
35 Morata, G. & Lawrence, P. A. Control of compartment development by the engrailed gene in Drosophila. *Nature* **255**, 614-617 (1975).
36 Crick, F. H. & Lawrence, P. A. Compartments and polyclones in insect development. *Science* **189**, 340-347 (1975).

37 Landsberg, K. P. *et al.* Increased cell bond tension governs cell sorting at the Drosophila anteroposterior compartment boundary. *Curr Biol* **19**, 1950-1955 (2009).
38 Dickson, A. D. The form of the mouse blastocyst. *J Anat* **100**, 335-348 (1966).
39 Corson, L. B., Yamanaka, Y., Lai, K. M. & Rossant, J. Spatial and temporal patterns of ERK signaling during mouse embryogenesis. *Development* **130**, 4527-4537 (2003).
40 Shahbazi, M. N. *et al.* Pluripotent state transitions coordinate morphogenesis in mouse and human embryos. *Nature* **552**, 239-243 (2017).
41 Frankenberg, S. *et al.* Primitive endoderm differentiates via a three-step mechanism involving Nanog and RTK signaling. *Dev Cell* **21**, 1005-1013 (2011).
42 Kunath, T. *et al.* Developmental differences in the expression of FGF receptors between human and mouse embryos. *Placenta* **35**, 1079-1088 (2014).
43 Zhang, Y. *et al.* Dynamic epigenomic landscapes during early lineage specification in mouse embryos. *Nat Genet* **50**, 96-105 (2018).
44 Ornitz, D. M. & Itoh, N. The Fibroblast Growth Factor signaling pathway. *Wiley Interdiscip Rev Dev Biol* **4**, 215-266 (2015).
45 Mason, F. M., Tworoger, M. & Martin, A. C. Apical domain polarization localizes actin-myosin activity to drive ratchet-like apical constriction. *Nat Cell Biol* **15**, 926-936 (2013).
46 Gardner, R. L. Investigation of cell lineage and differentiation in the extraembryonic endoderm of the mouse embryo. *J Embryol Exp Morphol* **68**, 175-198 (1982).
47 Salamat, M., Miosge, N. & Herken, R. Development of Reichert's membrane in the early mouse embryo. *Anat Embryol (Berl)* **192**, 275-281 (1995).
48 Latorre, E. *et al.* Active superelasticity in three-dimensional epithelia of controlled shape. *Nature* **563**, 203-208 (2018).
49 Butler, L. C. *et al.* Cell shape changes indicate a role for extrinsic tensile forces in Drosophila germ-band extension. *Nat Cell Biol* **11**, 859-864 (2009).
50 Wyatt, T. P. *et al.* Emergence of homeostatic epithelial packing and stress dissipation through divisions oriented along the long cell axis. *Proc Natl Acad Sci U S A* **112**, 5726-5731 (2015).
51 Christodoulou, N. *et al.* Sequential formation and resolution of multiple rosettes drive embryo remodelling after implantation. *Nat Cell Biol* **20**, 1278-1289 (2018).
52 Migeotte, I., Omelchenko, T., Hall, A. & Anderson, K. V. Rac1-dependent collective cell migration is required for specification of the anterior-posterior body axis of the mouse. *PLoS Biol* **8**, e1000442 (2010).
53 Yamaguchi, N., Mizutani, T., Kawabata, K. & Haga, H. Leader cells regulate collective cell migration via Rac activation in the downstream signaling of integrin beta1 and PI3K. *Sci Rep* **5**, 7656 (2015).
54 Fagotto, F. The cellular basis of tissue separation. *Development* **141**, 3303-3318 (2014).
55 Fagotto, F., Rohani, N., Touret, A. S. & Li, R. A molecular base for cell sorting at embryonic boundaries: contact inhibition of cadherin adhesion by ephrin/ Eph-dependent contractility. *Dev Cell* **27**, 72-87 (2013).
56 Calzolari, S., Terriente, J. & Pujades, C. Cell segregation in the vertebrate hindbrain relies on actomyosin cables located at the interhombomeric boundaries. *EMBO J* **33**, 686-701 (2014).
57 Rayon, T. *et al.* Notch and hippo converge on Cdx2 to specify the trophectoderm lineage in the mouse blastocyst. *Dev Cell* **30**, 410-422 (2014).

58 Watanabe, Y. *et al.* Notch and Hippo signaling converge on Strawberry Notch 1 (Sbno1) to synergistically activate Cdx2 during specification of the trophectoderm. *Sci Rep* **7**, 46135 (2017).
59 Rayon, T. *et al.* Distinct mechanisms regulate Cdx2 expression in the blastocyst and in trophoblast stem cells. *Sci Rep* **6**, 27139 (2016).
60 Furukawa, K. T., Yamashita, K., Sakurai, N. & Ohno, S. The Epithelial Circumferential Actin Belt Regulates YAP/TAZ through Nucleocytoplasmic Shuttling of Merlin. *Cell Rep* **20**, 1435-1447 (2017).
61 Martin, A. C., Kaschube, M. & Wieschaus, E. F. Pulsed contractions of an actin-myosin network drive apical constriction. *Nature* **457**, 495-499 (2009).
62 Lee, J. Y. & Harland, R. M. Actomyosin contractility and microtubules drive apical constriction in Xenopus bottle cells. *Dev Biol* **311**, 40-52 (2007).
63 Christodoulou, N. & Skourides, P. A. Cell-Autonomous Ca(2+) Flashes Elicit Pulsed Contractions of an Apical Actin Network to Drive Apical Constriction during Neural Tube Closure. *Cell Rep* **13**, 2189-2202 (2015).
64 Brown, J. M. & Garcia-Garcia, M. J. Secretory pathway calcium ATPase 1 (SPCA1) controls mouse neural tube closure by regulating cytoskeletal dynamics. *Development* **145** (2018).
65 Shraiman, B. I. Mechanical feedback as a possible regulator of tissue growth. *Proc Natl Acad Sci U S A* **102**, 3318-3323 (2005).
66 Pouille, P. A., Ahmadi, P., Brunet, A. C. & Farge, E. Mechanical signals trigger Myosin II redistribution and mesoderm invagination in Drosophila embryos. *Sci Signal* **2**, ra16 (2009).
67 Mitrossilis, D. *et al.* Mechanotransductive cascade of Myo-II-dependent mesoderm and endoderm invaginations in embryo gastrulation. *Nat Commun* **8**, 13883 (2017).
68 Kobb, A. B., Zulueta-Coarasa, T. & Fernandez-Gonzalez, R. Tension regulates myosin dynamics during Drosophila embryonic wound repair. *J Cell Sci* **130**, 689-696 (2017).
69 Liu, P., Jenkins, N. A. & Copeland, N. G. A highly efficient recombineering-based method for generating conditional knockout mutations. *Genome Res* **13**, 476-484 (2003).
70 Adams, D. J. *et al.* A genome-wide, end-sequenced 129Sv BAC library resource for targeting vector construction. *Genomics* **86**, 753-758 (2005).
71 van der Weyden, L. *et al.* Null and conditional semaphorin 3B alleles using a flexible puroDeltatk loxP/FRT vector. *Genesis* **41**, 171-178 (2005).
72 Magin, T. M., McWhir, J. & Melton, D. W. A new mouse embryonic stem cell line with good germ line contribution and gene targeting frequency. *Nucleic Acids Res* **20**, 3795-3796 (1992).
73 Rodriguez, C. I. *et al.* High-efficiency deleter mice show that FLPe is an alternative to Cre-loxP. *Nat Genet* **25**, 139-140 (2000).
74 Live imaging of mouse embryos during pre-implantation and peri-implantation development. Protocol Exchange (2019) DOI: 10.21203/rs.2.10053/v1

Author Contributions

N.C and A.W designed and carried out the experiments and data analysis. D.S, K. I.A, and P. T generated the E-cadherin-GFP transgenic line. N.C, A.W and M.Z-G wrote the manuscript. M.Z-G conceived and supervised the project with the help of N.C.

Acknowledgments

We are grateful to D. Glover, M. Shahbazi, M. Zhu and C. Kyprianou for feedback on the manuscript. The M.Z.G lab is supported by grants from the European Research Council (669198) and the Welcome Trust (098287/Z/12/Z) and the EU Horizon 2020 Marie Sklodowska-Curie actions (ImageInLife,721537).

Competing Interests

The authors declare no competing interests.

Figure legends

Figure 1. Polar trophectoderm transformation. (a) Schematic for blastocyst to egg cylinder transformation. (b) Embryos at late pre-implantation blastocyst (E4.5) and early egg cylinder (E5.0-E5.25) stages stained for markers for primitive endoderm (PE)/visceral endoderm (VE) (Gata6) and trophectoderm (TE)/extra-embryonic ectoderm (ExE) (Cdx2). Representative of 20 embryos for each stage. (c) Embryo at peri-implantation stage (E4.75-E5.0). Polar trophectoderm (pTE) expansion to form the ExE (red outline) precedes PE spreading (white outlines) during blastocyst to egg cylinder transition. Representative of 20 embryos. (d) Stills from a time lapse movie of a Cdx2-GFP E3.5 blastocyst showing flow of cells from polar to mural TE. Cyan dots: tracking of individual cell nuclei. (e) Colour coded cell tracks according to number of generations as extracted after single cell tracking from Supplementary Movie 1 (d). Cyan dots: polar TE cells. Grey dots: mural TE cells. (f) Displacement map extracted after single cell tracking from Supplementary Movie 1 (d). (g) Polar TE displacement map extracted after single cell tracking from Supplementary Movie 1 (d). (h) Stills from a time lapse movie of Cdx2-GFP E4.5 implanting blastocyst combined with the displacement map (magenta: polar TE; white: mural TE) showing stop of cell flow from polar to mural TE upon implantation. (i) Stills from a time lapse movie of Cdx2-GFP E4.5 implanting blastocyst combined with single cell tracking (magenta: polar TE; cyan:

mural TE) showing stop of cell flow from polar to mural TE upon implantation. (j) Model of polar TE cell flow in pre- and post- implantation blastocysts. Scale bars = 20um.

Figure 2: Establishment of tissue boundary within the trophectoderm. (a) Maximum intensity projection (MIP) image of an implanted E4.75 blastocyst. Arrowheads indicate tissue boundary between polar and mural TE. Representative example of 20 embryos. (b) MIP image of an implanted E4.75 blastocyst. Arrowheads indicate actomyosin enrichment at the boundary between polar and mural TE. Representative example of 8 embryos. (c) Stills from a time lapse movie of Cdx2/E-Cad GFP E4.5 implanting blastocyst. Red line follows the boundary between high-Cdx2 cells (polar TE) and low-Cdx2 cells (mural TE). As development progresses, polar and mural TE cells segregate and a linear tissue boundary formed (arrowheads). (d) Quantification of cell-cell junction angle at the polar/mural TE boundary and within polar TE. Two-sided unpaired student's t-test; ****P<0.0001; mean±SEM. n=56 polar/mural TE and 63 polar TE cell junctions. Source data are provided as a Source Data file. Scale bars=20um

Figure 3: Cell shape changes and polarized cell divisions drive polar TE expansion (a) Stills from a time-lapse movie of Lifeact-GFP blastocyst. Red arrowheads indicate the polar/mural TE boundary. Boundary formation is followed by polar TE expansion. (b) Quantification of polar TE cell aspect ratio at different developmental stages. Two-sided unpaired student's t-test; ****P<0.0001; mean±SEM. Pre-implantation blastocyst: n=216 cells; Implanted blastocyst: n=152 cells; Transitioning blastocyst; n=75 cells. (c) Quantification of polar TE apical cell surface are. Two-sided unpaired student's t-test; ****P<0.0001; mean±SEM. Blastocyst before: n=186 cells; Transitioning blastocyst; n=163 cells. (d) Stills from a time lapse movie of Lifeact-GFP implanted blastocyst. Polar TE expansion is evident at 2.5h upon polar TE cell shape changes and polarised cell division. (e) Representative examples of polar TE cells dividing parallel to Embryonic(Em)/Abembryonic(Ab) axis during polar TE expansion. (f) Rose diagram for quantification of cell division orientation in blastocysts before (green) and during (purple) polar TE expansion. Kolmogorov-Smirnov test: ****p<0.0001. Blastocyst before polar TE expansion: n= 24, Bastocyst during polar TE expansion: n= 36. Source data are provided as a Source Data file.Scale bars= 20um.

Figure 4. Tissue boundary is necessary for polar trophectoderm expansion.

(a) Implanted blastocyst (E4.75) stained for phosphorylated ERK (pERK). pERK is detected in the primitive endoderm (PE) and the trophectoderm (TE). pERK is restricted to the polar region of the TE. (b) Implanted blastocyst (E4.75) stained for phosphorylated AKT (pAKT). pAKT is restricted to the polar region of the TE. For (a) and (b) representative example of 10 embryos. (c) Schematic representation of the experimental design to examine the contribution of actomyosin contractility and FGF signalling in the formation of polar/mural TE tissue boundary formation. (d) Representative examples of control, Y27632 (ROCK inhibitor) and SU5402 (Fgfr inhibitor) treated blastocysts cultured as described in (c) and analysed for the presence of polar/mural TE boundary (cyan dotted line). Polar/mural tissue boundary formation is defective in the absence of actomyosin contractility and FGF signalling. (e) Quantification of polar/mural TE boundary formation efficiency in control, Y27632 and SU5402 treated blastocysts. χ^2 test ; ****P<0.0001, mean±SEM. For (d) and (e) FGF n= 29 control, 15 Y27632 treated and 15 SU5402 treated embryos. (f) Quantification of cell-cell junction angles at the polar/mural TE interface. The angles of junctions after abrogation of actomyosin contractility (Y27632) and signalling (SU5402) are narrowed in agreement with the defective formation of polar/mural TE tissue boundary in these conditions. Two-sided unpaired student's t-test; ****P<0.0001; mean±SEM. Control: n=57; Y27632: n=38; SU5402: n=45. (g) Representative examples of control, Y27632 (ROCK inhibitor) and SU5402 (FGFR inhibitor) treated blastocyst cultured as described in (b) and analysed for polar-TE (white outline) expansion. (h) Quantification polar TE expansion efficiency in control, Y27632 and SU5402 treated blastocysts. χ^2 test ; ****P<0.0001. For (f) and (g) n= 29 control, 15 Y27632 treated and 15 SU5402 treated embryos. (i) Model for the molecular and cellular events necessary for polar TE expansion during peri-implantation morphogenesis. Source data are provided as a Source Data file. Scale bars= 20um

Figure 5. Primitive endoderm behaviour during the blastocyst to egg cylinder transition. (a) Examples of embryos used for analysis of primitive endoderm (PE) cell shape at different stages of peri-implantation development. Representative of 20 embryos for each stage. (b) Quantification of PE cell aspect ratio at different developmental stages. The red lines between different columns correspond to events taking place within the trophectoderm (TE). Two-sided unpaired student's t-test; ****P<0.0001; mean±SEM. Pre-implantation blastocyst: n=117 cells; Implanted blastocyst: n=219 cells; Transitioning blastocyst: n=117 cells; early egg cylinder: n=184 cells. (c) Stills from a time lapse movie of Lifeact-GFP E4.5 implanting blastocyst. PE (cyan) acquires a columnar morphology at implantation stages and

this is followed by tissue spreading through cell-shape changes upon polar-TE (red) expansion as quantified in (b). Red double-headed arrows: polar TE expansion. Cyan arrows: PE spreading. Stills without coloured overlay are presented in Supplementary Figure 7b. (d) Representative examples of implanting blastocyst (E4.5-E4.75). Parietal endoderm migration is completed before the expansion of the TE (double headed arrows in bottom row) and before PE (red outline in 2D images) spreading over the lateral sides of the epiblast (bottom row). Red arrows indicate the front of the migrating parietal endoderm. (e) Representative examples of transitioning blastocysts (E5.0) displaying expanded polar trophectoderm and early egg cylinders. Primitive endoderm cells are found enclosed between the embryonic and Reichert's basement membrane during blastocyst to egg-cylinder transformation. arrowheads: Reichert's membrane. Arrows: Embryonic basement membrane. Dots: Proximal cells. Representative images of 20 embryos per stage. Source data are provided as a Source Data file. Scale bars=20um

Figure 6. Trophectoderm folding orchestrates the final step the blastocyst to egg cylinder transformation.

(a) Stills from a time lapse movie of Lifeact-GFP blastocyst. ExE tissue (red) folding (white arrows) through apical constriction is followed by spreading (yellow arrows) of the visceral endoderm (VE) (yellow outline) and formation of egg cylinder. Stills without coloured overlay are presented in Supplementary Figure 10a. (b) Quantification of ExE apical cell surface area, VE apical cell surface area and VE length through time during blastocyst to egg cylinder transformation from 3 individual embryos shown in Supplementary Movie 8. Cyan boxes indicate the developmental period, during which ExE cell's apical constriction precedes VE spreading. VE tissue spreading during egg cylinder formation is due to cell-shape changes as quantified in Figure 5b. (c) Quantification of polar TE/ExE apical cell surface area relative to PE/VE position. (d) Quantification of PE/VE cell aspect ratio relative to PE/VE position. (e) Quantification of PE/VE cell aspect ratio relative to polar-TE/ExE apical cell surface area. (f) Quantification of polar TE/ExE cell aspect ratio relative to PE/VE cell aspect ratio. For c-f, Pearson correlation test was used, ****$p<0.0001$. (g) Rose diagram for quantification of long cell axis orientation in distal and proximal VE at the early egg cylinder stage. Kolmogorov-Smirnov test: ****$p<0.0001$. Distal VE: n= 153 cells, Proximal VE: n= 75 cells. (h) Representative examples of control and Y27632 (ROCK inhibitor) treated embryos. Embryos were recovered at E4.75 and cultured ex-vivo for 12 hours. In the

absence of actomyosin contractility (Y27632) egg cylinder formation fails due to defective ExE folding (Supplementary Movie 10). (i) Quantification of blastocyst to egg cylinder transformation efficiency in control, and Y27632 treated embryos. χ^2 test ; ****P<0.0001. For (h) and (i) n=16 control and 29 Y27632 treated embryos. (j) Model of blastocyst to egg cylinder transformation as a result of TE morphogenesis. Source data are provided as a Source Data file. Scale bars=20um.

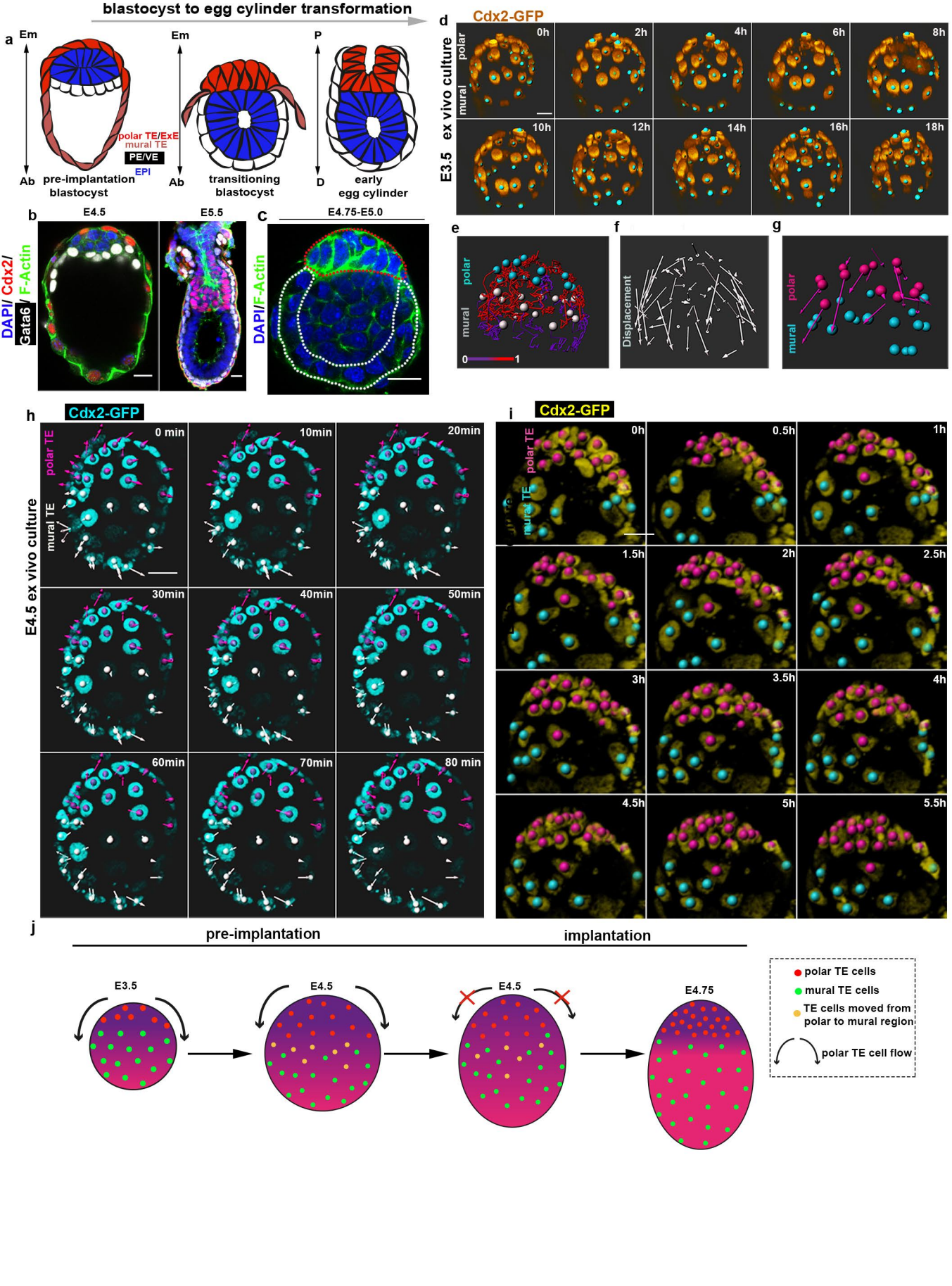
blastocyst to egg cylinder transformation
a
Em
Ab
pre-implantation blastocyst
polar TE/ExE
mural TE
PE/VE
EPI
transitioning blastocyst
P
D
early egg cylinder
d
Cdx2-GFP
E3.5 ex vivo culture
polar
mural
0h
2h
4h
6h
8h
10h
12h
14h
16h
18h
b
E4.5
E5.5
DAPI/ Cdx2/ Gata6/ F-Actin
c
E4.75-E5.0
DAPI/F-Actin
e
f
Displacement
g
h
Cdx2-GFP
E4.5 ex vivo culture
polar TE
mural TE
0 min
10min
20min
30min
40min
50min
60min
70min
80 min
i
Cdx2-GFP
0h
0.5h
1h
1.5h
2h
2.5h
3h
3.5h
4h
4.5h
5h
5.5h
j
pre-implantation
implantation
E3.5
E4.5
E4.5
E4.75
polar TE cells
mural TE cells
TE cells moved from polar to mural region
polar TE cell flow

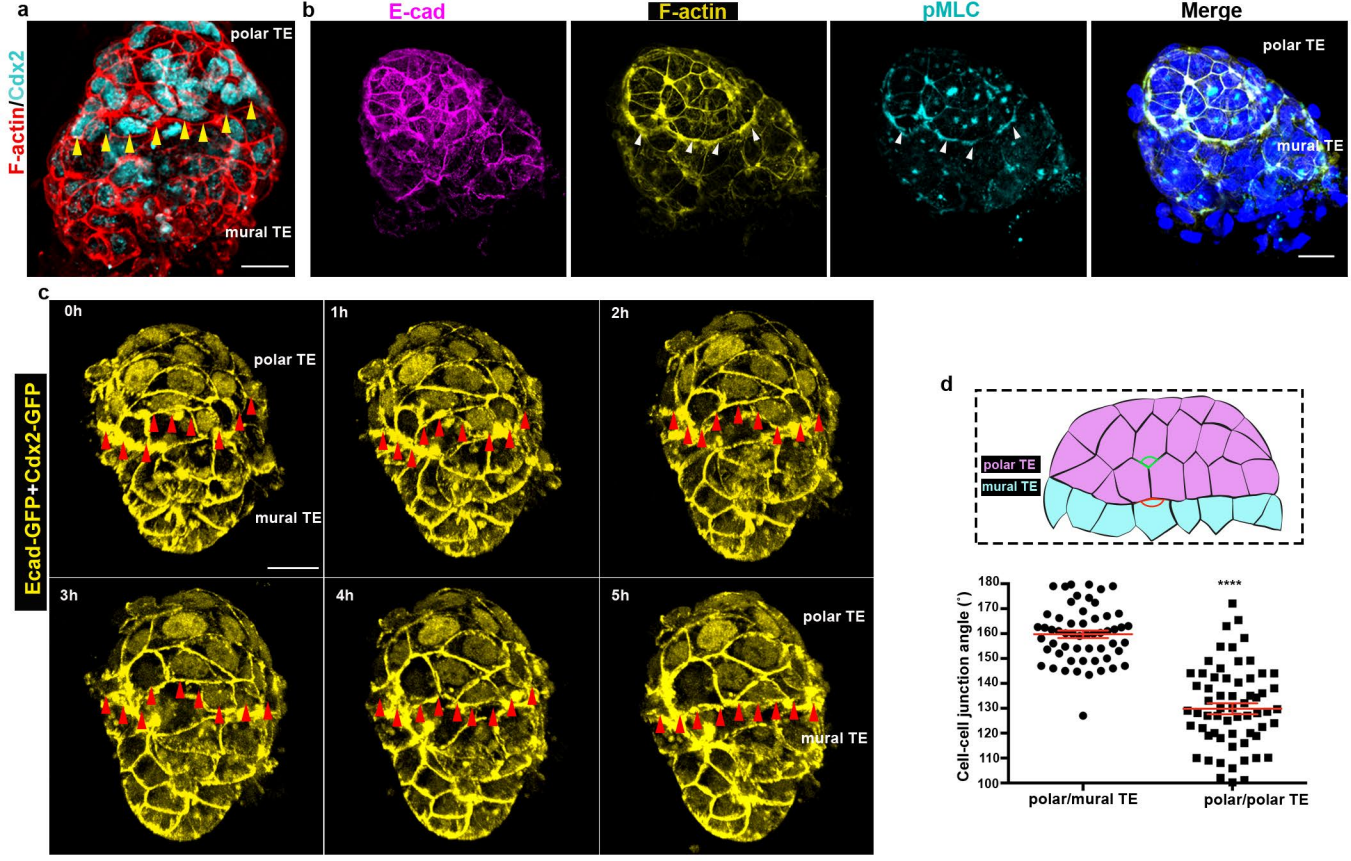
a
F-actin/Cdx2
polar TE
mural TE
b
E-cad
F-actin
pMLC
Merge
polar TE
mural TE
c
Ecad-GFP+Cdx2-GFP
0h
1h
2h
3h
4h
5h
polar TE
mural TE
d
polar TE
mural TE
Cell-cell junction angle (°)
180
170
160
150
140
130
120
110
100
****
polar/mural TE
polar/polar TE

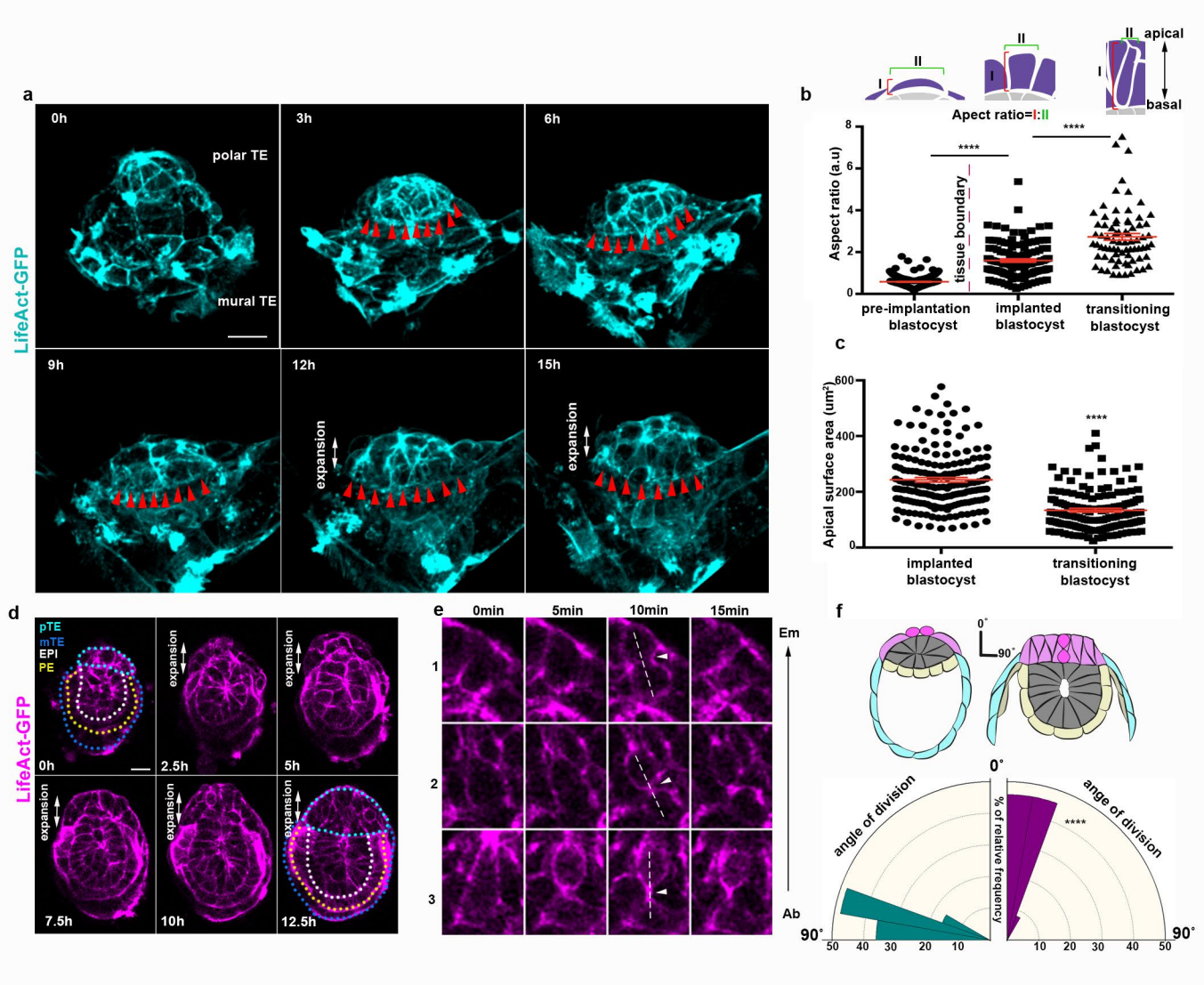
a
LifeAct-GFP
0h
polar TE
mural TE
3h
6h
9h
12h
expansion
15h
expansion
b
I
II
apical
basal
Apect ratio=I:II
Aspect ratio (a.u)
tissue boundary
****
****
pre-implantation blastocyst
implanted blastocyst
transitioning blastocyst
c
Apical surface area (um²)
****
implanted blastocyst
transitioning blastocyst
d
LifeAct-GFP
pTE
mTE
EPI
PE
0h
2.5h
5h
7.5h
10h
12.5h
expansion
e
0min
5min
10min
15min
1
2
3
Em
Ab
f
0˚
90˚
angle of division
angle of division
% of relative frequency
****
90˚
90˚
50 40 30 20 10
10 20 30 40 50

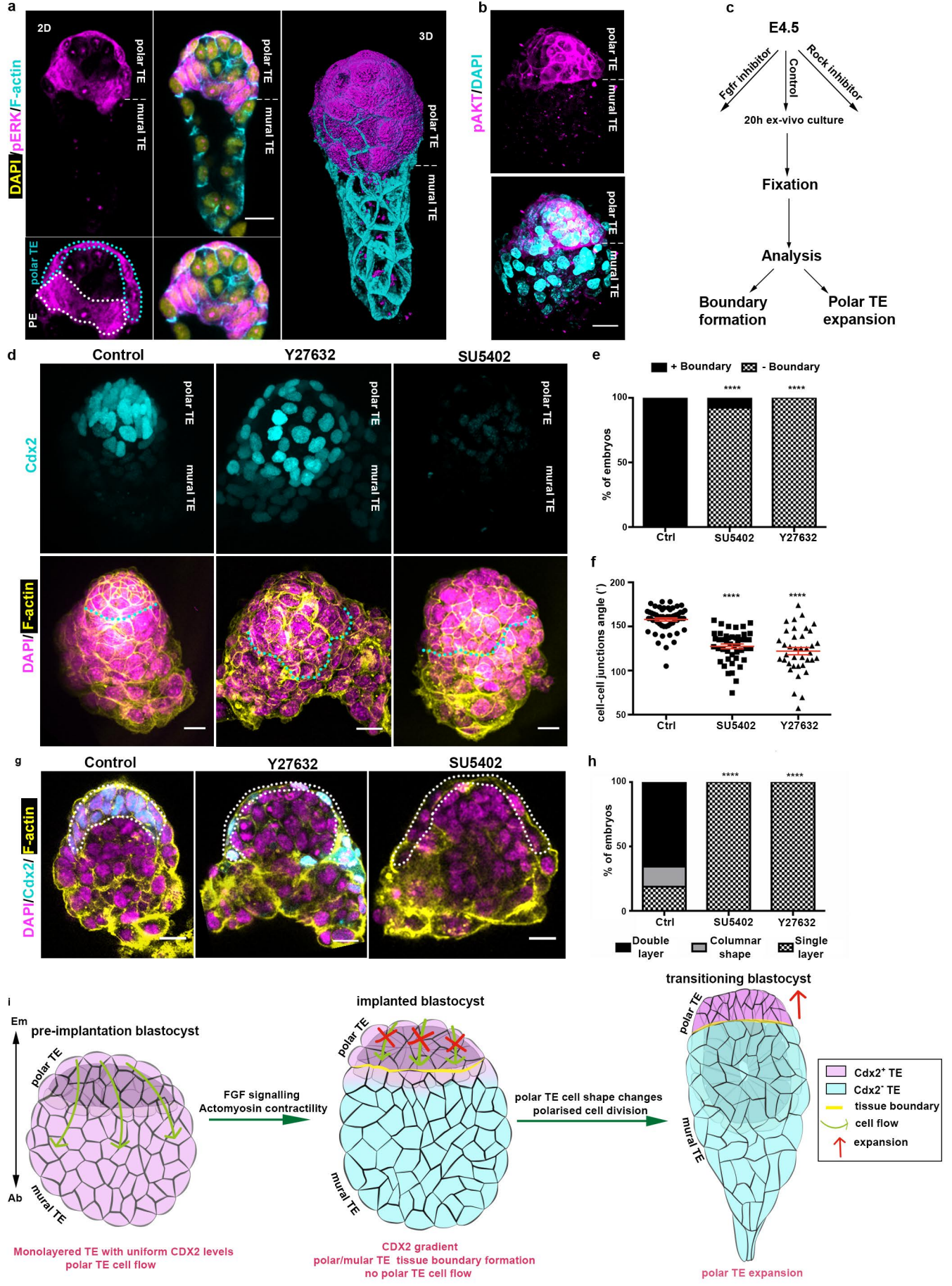
a
2D
3D
DAPI/pERK/F-actin
polar TE
mural TE
PE
b
pAKT/DAPI
c
E4.5
Fgfr inhibitor
Control
Rock inhibitor
20h ex-vivo culture
Fixation
Analysis
Boundary formation
Polar TE expansion
d
Control
Y27632
SU5402
Cdx2
DAPI/F-actin
e
+ Boundary
- Boundary
% of embryos
Ctrl
SU5402
Y27632
****
f
cell-cell junctions angle (°)
g
DAPI/Cdx2/F-actin
h
Double layer
Columnar shape
Single layer
i
pre-implantation blastocyst
implanted blastocyst
transitioning blastocyst
Em
Ab
FGF signalling
Actomyosin contractility
polar TE cell shape changes
polarised cell division
Cdx2+ TE
Cdx2- TE
tissue boundary
cell flow
expansion
Monolayered TE with uniform CDX2 levels
polar TE cell flow
CDX2 gradient
polar/mular TE tissue boundary formation
no polar TE cell flow
polar TE expansion

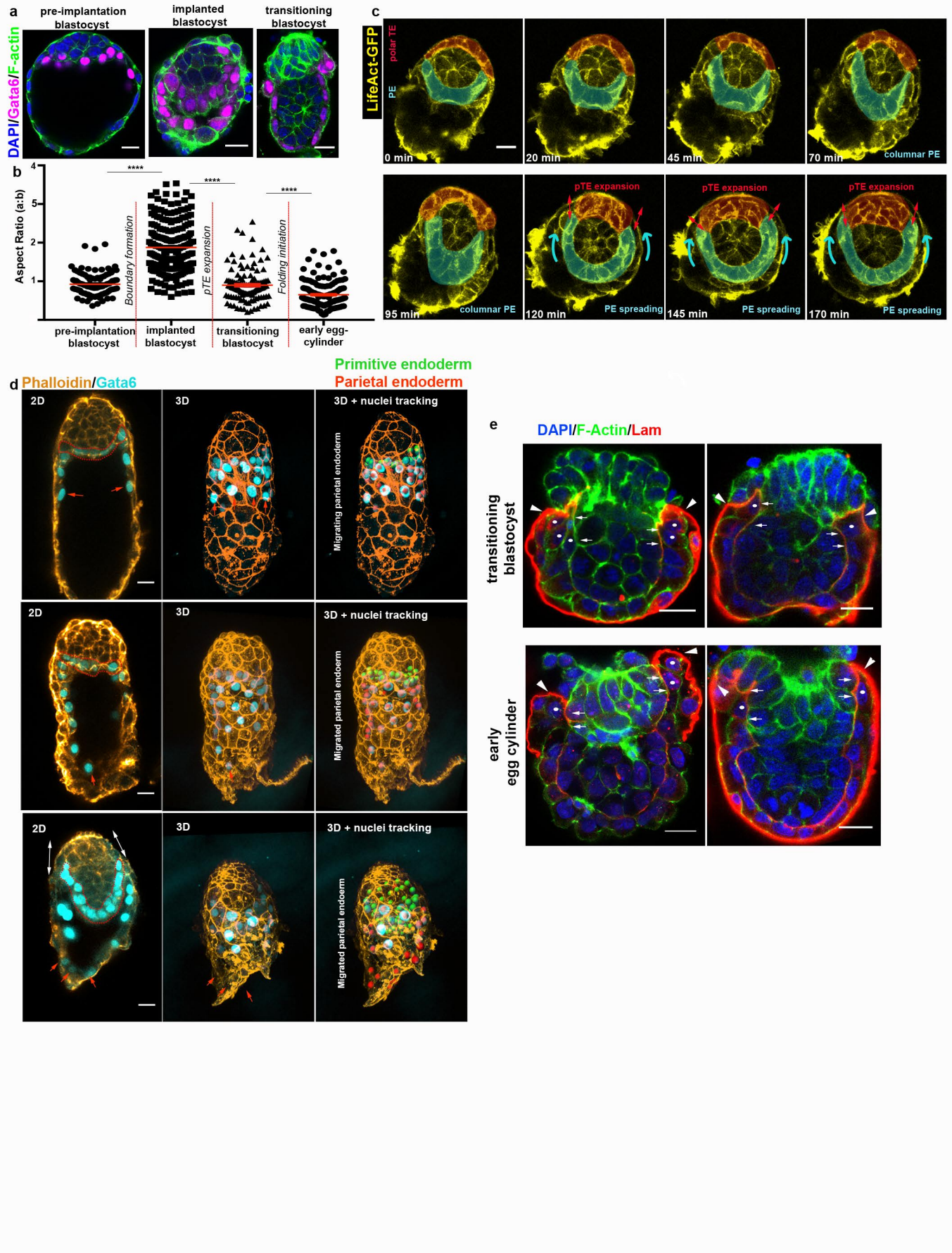
a
pre-implantation blastocyst
implanted blastocyst
transitioning blastocyst
DAPI/Gata6/F-actin
b
Aspect Ratio (a:b)
Boundary formation
pTE expansion
Folding initiation
****
pre-implantation blastocyst
implanted blastocyst
transitioning blastocyst
early egg-cylinder
c
LifeAct-GFP
polar TE
PE
0 min
20 min
45 min
70 min
columnar PE
95 min
columnar PE
120 min
pTE expansion
PE spreading
145 min
pTE expansion
PE spreading
170 min
pTE expansion
PE spreading
d
Phalloidin/Gata6
Primitive endoderm
Parietal endoderm
2D
3D
3D + nuclei tracking
Migrating parietal endoderm
Migrated parietal endoerm
Migrated parietal endoerm
e
DAPI/F-Actin/Lam
transitioning blastocyst
early egg cylinder

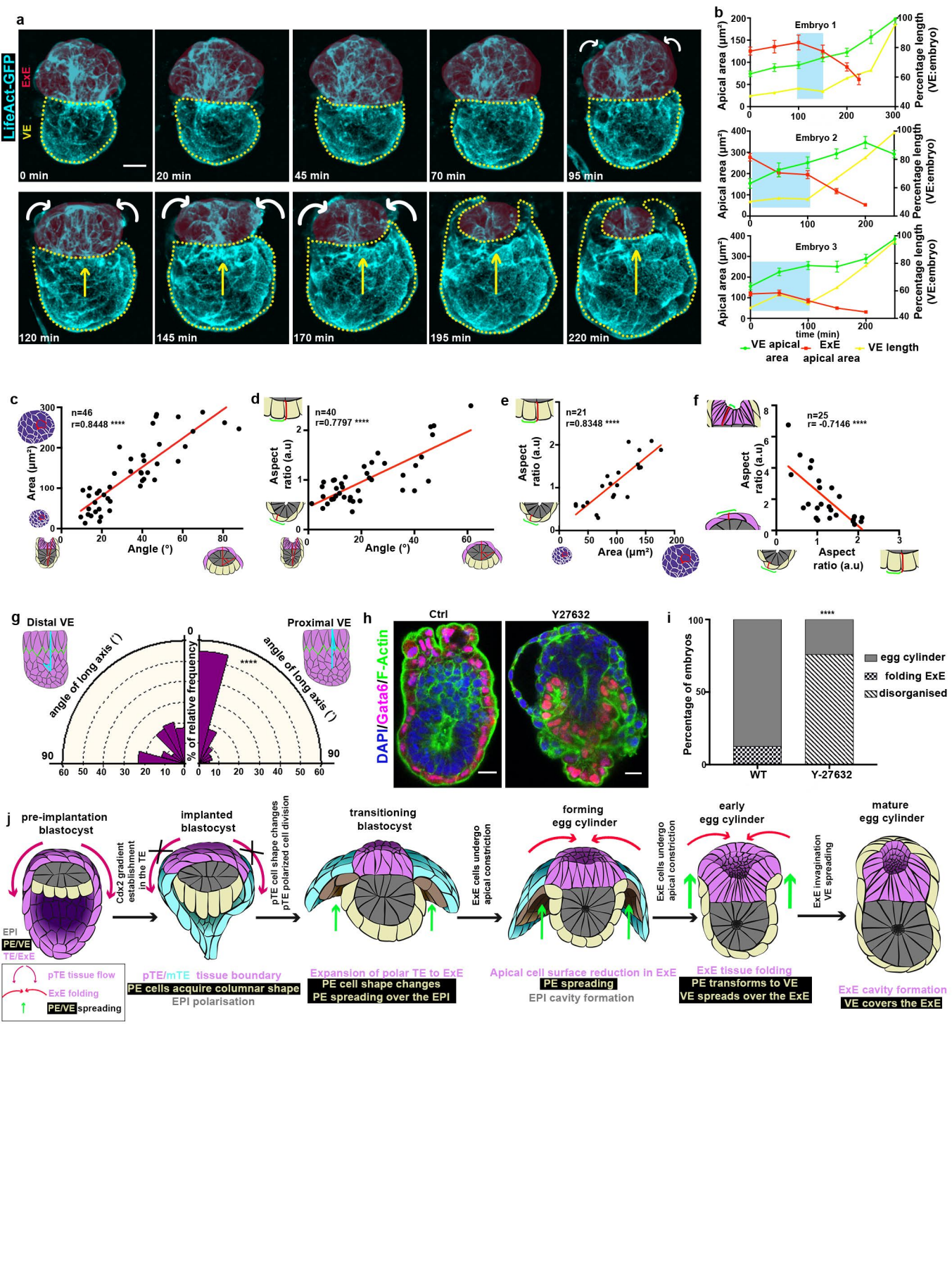
a
LifeAct-GFP
ExE
VE
0 min
20 min
45 min
70 min
95 min
120 min
145 min
170 min
195 min
220 min
b
Embryo 1
Embryo 2
Embryo 3
Apical area (µm²)
Percentage length (VE:embryo)
time (min)
VE apical area
ExE apical area
VE length
c
n=46
r=0.8448 ****
Area (µm²)
Angle (°)
d
n=40
r=0.7797 ****
Aspect ratio (a.u)
Angle (°)
e
n=21
r=0.8348 ****
Aspect ratio (a.u)
Area (µm²)
f
n=25
r= -0.7146 ****
Aspect ratio (a.u)
Aspect ratio (a.u)
g
Distal VE
Proximal VE
angle of long axis (°)
% of relative frequency
****
h
Ctrl
Y27632
DAPI/Gata6/F-Actin
i
Percentage of embryos
****
egg cylinder
folding ExE
disorganised
WT
Y-27632
j
pre-implantation blastocyst
implanted blastocyst
transitioning blastocyst
forming egg cylinder
early egg cylinder
mature egg cylinder
Cdx2 gradient establishment in the TE
pTE cell shape changes pTE polarized cell division
ExE cells undergo apical constriction
ExE cells undergo apical constriction
ExE invagination VE spreading
EPI
PE/VE
TE/ExE
pTE tissue flow
ExE folding
PE/VE spreading
pTE/mTE tissue boundary
PE cells acquire columnar shape
EPI polarisation
Expansion of polar TE to ExE
PE cell shape changes
PE spreading over the EPI
Apical cell surface reduction in ExE
PE spreading
EPI cavity formation
ExE tissue folding
PE transforms to VE
VE spreads over the ExE
ExE cavity formation
VE covers the ExE